

Dirac plasmon polaritons and magnetic modes in topological-insulator nanoparticles

Nikolaos Kyvelos ^{1,*}, Vassilios Yannopoulos ², N. Asger Mortensen ^{1,3} and Christos Tserkezis ^{1,†}

¹*POLIMA—Center for Polariton-driven Light–Matter Interactions,
University of Southern Denmark, Campusvej 55, DK-5230 Odense M, Denmark*

²*Department of Physics, School of Applied Mathematical and Physical Sciences,
National Technical University of Athens, GR-15780 Athens, Greece*

³*Danish Institute for Advanced Study, University of Southern Denmark, Campusvej 55, DK-5230 Odense M, Denmark*

(Dated: May 21, 2024)

We demonstrate the existence of previously unreported magnetic modes with record-high magnetic Purcell factors in topological-insulator nanospheres. Focusing on bismuth selenide (Bi_2Se_3), and based on full electromagnetic Mie theory, we find magnetic modes arising from both displacement current loops in the bulk, and surface currents due to delocalized surface states, induced by electronic transitions between topologically protected states within the Dirac cone and discretized due to the sphere finite size. Furthermore, we discuss how Dirac plasmon polaritons, resulting from the interaction between THz photons and Dirac electrons, dramatically influence both the magnetic and the electric transitions of quantum emitters placed near Bi_2Se_3 nanospheres, significantly enhancing the corresponding Purcell factors. These findings position Bi_2Se_3 nanospheres, whose optical response is related to a richness of physical mechanisms, among the most promising candidates for enhancing light–matter interactions in nanophotonics and THz technologies.

I. INTRODUCTION

Achieving strong coupling between light and atoms is one of the main focuses of quantum optics [1], and has inspired nanophotonics to enter a quest for confining electromagnetic (EM) modes within the smallest possible volume, aiming to enhance light–matter interactions in the visible and infrared [2, 3]. To this end, plasmonics, with its tremendous field enhancement and confinement, offers a natural template [4–9]. However, the inherent Ohmic losses in noble metals [10, 11] tend to hinder their exploitation in quantum technologies, and efforts have been made to identify alternatives, e.g. in high-index dielectrics [12, 13]. Dielectrics host EM states (Mie resonances) of both electric and magnetic character which, on some occasions, dominate the frequency window of interest [14, 15], and provide flexibility in tailoring the decay rate of quantum emitters (QEs) [16]. Therefore, they offer the possibility of controlling magnetic transitions of atoms via the magnetic Purcell effect [17, 18]. Although the Purcell effect was originally associated with magnetic transition in atoms [19], most studies so far, both with plasmonic and dielectric photonic environments, focus on electric-dipole QEs; ways of achieving strong light–matter interactions with magnetic-dipole QEs are still limited [20].

Topological insulators (TIs) [21] have emerged in the last couple of decades as prominent candidates for applications in both quantum technologies [22–24] and topological photonics [25–27]. The latter area is practically divided into two subfields dominated by different physics. One is related to the exploration of photonic EM states endowed with topological protection [28, 29], as observed in photonic-crystal architectures inspired by solid-state systems [30–32], mainly as a result of time-reversal symmetry [33–35]. The other involves electronic topological systems interacting with light [36, 37]. In this work, we

focus solely on the second situation, where the topological phenomena are embodied in the electronic structure of the host material. Specifically, we theoretically investigate the manipulation of Dirac plasmon polaritons (DPPs) [38–40] hosted within Bi_2Se_3 spherical nanoparticles (NPs), with the aim of controlling the spontaneous emission of QEs. In this context, DPPs represent EM eigenstates that arise from the collective coupling of massless Dirac electrons [41] residing on the surface of a TI.

Apart from DPPs, further opportunities for exploitation of TIs in photonics emerge when molding them into nanostructures. In a previous work [42], an in-depth analysis on the electronic spectrum of a spherical TI of nanometer dimensions revealed quantization of the surface states within the Dirac cone of the electronic band structure. This finding was subsequently analyzed in terms of its influence on the NP optics [43], where transitions between these discrete levels were shown to induce a surface charge density manifesting in the optical spectra as what was termed a surface topological particle (SToP) mode. Nevertheless, this response has only been studied so far within the quasistatic regime [44]. Here, we seek to identify what effects are ignored in such a description. In particular, by employing fully electrodynamic Mie-theory-based calculations, we ask what happens when one considers the dynamics of this surface charge density, and whether the resulting surface current can lead to magnetic optical response. At the same time, since TIs are usually characterized by very large permittivities, we investigate the possible emergence of magnetic modes as a result of displacement currents, in analogy with traditional Mie-resonant semiconductors such as silicon [45, 46]. Focusing on Bi_2Se_3 NPs, we demonstrate previously unreported EM states of magnetic nature spanning over a wide window in the THz regime, and show that these states are capable of strongly af-

fecting atomic transitions over a wide range of NP–atom distances and frequencies. The magnetic Purcell factors (PFs) predicted in this work are among the highest reported in literature, potentially enabling the control of otherwise forbidden transitions [47]. We anticipate that our work will trigger a further quest for artificial atoms with transitions in the THz regime [48, 49], or for ways to engineer TI NPs so as to push their optical response towards the visible.

II. METHODOLOGY

The electronic configuration of TIs, in both two and three dimensions, exhibits energy band gaps within the bulk, while featuring gapless edge or surface states, usually characterized by a Dirac dispersion [50] [see sketch in Fig. 1(a)]. Much like the case of graphene [51–53], these topological surface states accommodate massless Dirac electrons confined within a two-dimensional (2D) domain. The surface states demonstrate strong spin–momentum coupling, resulting in remarkable suppression of backscattering, as a direct consequence of time-reversal symmetry [54]; electrons cannot backscatter between distinct surface states unless there is a concurrent spin-flip event. The outcome of this behavior is the emergence of unidirectional surface currents [55, 56]. In a three-dimensional (3D) TI [57, 58], the surface states are characterized by an odd number of Dirac cones—in the simplest scenario a single one [59]. Among TIs, Bi_2Se_3 stands out for its relatively high bulk band gap of 0.3 eV, featuring a single Dirac cone within its surface states. This substantial band gap is attributed to the robust spin–orbit coupling, arising from the presence of the heavy bismuth element [60]. Upon reduction to nanoscale structures, the escalating surface-to-volume ratio intuitively leads to the anticipation that surface-related phenomena will significantly impact the electrical and optical characteristics of the material. Spin–momentum locking [61] of electrons within the TI surface states opens possibilities for applications in THz sensing [62, 63], spintronics [64] and for distinct phenomena such as spin-polarized plasmon waves [65, 66].

As discussed above, the transition from bulk to a nanostructured TI comes with a natural, yet significant implication: the surface states become quantized, leading to discrete energy levels encompassed by the Dirac cone of the electronic band structure [42]. These energy levels are equidistant, and located symmetrically around the zero of the energy axis (Dirac point), at intervals of $\Delta\mathcal{E} = A/R$, where R denotes the NP radius. The parameter A represents the spin–orbit coupling strength, with density-functional theory (DFT) predicting a value of 0.3 eV nm in the case of Bi_2Se_3 [67]. The resulting spacing of surface states is of the order of THz, highlighting thus the potential of TI NPs to bridge the so-called THz gap [68, 69] and bring photonic systems closer to electronic ones. In what follows, we assume that all occu-

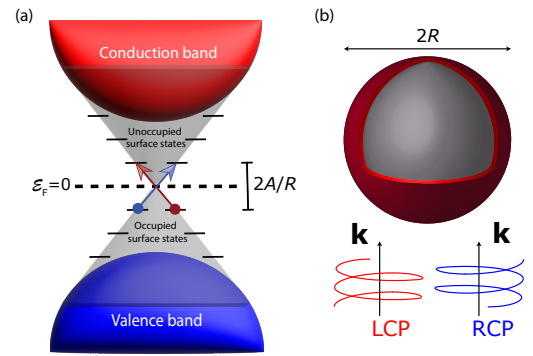


FIG. 1. (a) Sketch of the band structure of a TI, with a band gap between the valence and conduction bands, and a Dirac cone corresponding to surface states. In small NPs, the surface Dirac cone exhibits discrete energy levels, with energy spacing $\Delta\mathcal{E} = A/R$, where A quantifies the spin–orbit coupling strength. We assume that the Fermi energy \mathcal{E}_F is at the Dirac point. The color arrows indicate allowed transitions between occupied and unoccupied surface states. (b) A spherical Bi_2Se_3 NP of radius R , excited by two oppositely-handed circularly-polarized plane waves of wavevector \mathbf{k} . Transitions between occupied and unoccupied states lead to electronic surface states that manifest in the optics as a surface current, sketched as an infinitesimally thin shell.

ried energy states extend up to the Dirac point, implying that transitions occur from the lower to the upper part of the Dirac cone, as illustrated in Fig. 1(a). The charge density that corresponds to interband transitions in the Dirac cone can be calculated within time-dependent perturbation theory [43] in the dipole approximation. To address the optics of an NP with such surface charges, in a zero-order approach one can incorporate the resulting surface charge density into the NP polarizability, via an angular frequency (ω)-dependent function $\delta_R(\omega)$, given as

$$\delta_R(\omega) = \frac{e^2}{6\pi\epsilon_0 R} \left(\frac{1}{2\Delta\mathcal{E} - \hbar\omega} + \frac{1}{2\Delta\mathcal{E} + \hbar\omega} \right). \quad (1)$$

This term originates from transitions occurring between the delocalized topologically-protected surface states, which are perturbed by two oppositely-handed, left- and right-circularly polarized (LCP/RCP) waves, as sketched in Fig. 1(b). It should be noted that, formally, this expression does not adhere to causality, as it lacks an imaginary part, since it does not take into account the lifetime of the transitions between surface states; towards the end of the paper, we will address this issue in a qualitative but still phenomenological way.

Introducing Eq (1) into the quasistatic polarizability, the absorption cross section of a small nanosphere becomes

$$\sigma_{\text{abs}}(\omega) = 4\pi R^3 \frac{2\pi}{\lambda} \text{Im} \left[\frac{\varepsilon_1 + \delta_R(\omega) - 1}{\varepsilon_1 + \delta_R(\omega) + 2} \right], \quad (2)$$

where λ is the wavelength of the incident light, ε_1 is the

relative permittivity of bulk Bi₂Se₃, and the NP environment has been assumed to be air. This is a reasonable starting point for studying the optical response of a system when the NP size is much smaller than the wavelength of the incident field, i.e., when the quasistatic approximation applies. The denominator of this expression implies that a singularity should occur when $\varepsilon_1 + \delta_R(\omega) + 2 = 0$ and, indeed, a sharp resonance attributed to the SToP mode has been theoretically predicted [43] and experimentally confirmed [44].

In what follows, we examine the system within a fully electrodynamic picture, aiming to serve a dual purpose: on the one hand, since it is known that high-refractive-index dielectrics sustain both electric and magnetic Mie resonances, the latter caused by displacement current loops in the bulk of the NP, we wish to explore whether these are relevant in the case of Bi₂Se₃. On the other hand, in a dynamic picture, the surface charge of Eq. (1) should be seen as a topological surface current, possibly leading to magnetic response as well. In addition, when studying the interaction of QEs with photonic resonators, higher-order multipoles are known to be of vital importance [70]. Going beyond the quasistatic approximation enables thus to capture the full range of optical modes of the system, and more accurately predict its coupling to QEs. We should stress here that there are two levels of dipole approximations in such a study; one concerning the possible transitions within the Dirac cone, which predicts the surface charge density that we use throughout the manuscript, and one concerning the optical response of the NP, once such a charge is placed on its surface. The former is only related to microscopic selection rules, and there is no obvious reason to depart from it.

Based on Mie theory [71], it is possible to calculate the scattering and absorption cross sections of Bi₂Se₃ nanospheres excited by a monochromatic plane wave. The NP is placed in vacuum, ensuring that the topologically non-trivial bulk is interfaced by a topologically trivial background. The modification in topological invariant at the interface necessitates the closure of the band gap, while simultaneously preserving the gap within the bulk of both media. This configuration leads to the manifestation of a topological phase transition at the NP surface, thereby revealing the emergence of conductive topological surface states. In the multipolar expansions of the incident, internal, and scattered fields in spherical waves, we use appropriate expansion coefficients $a_{P\ell m}^0$, $a_{P\ell m}^{\text{in}}$, and $a_{P\ell m}^+$, respectively. Here, the subscripts ℓ and m correspond to the usual angular momentum indices, while the polarization index $P = E, H$ refers to transverse electric (TE) or transverse magnetic (TM) polarization, respectively.

The expansion coefficients are determined by application of the appropriate boundary conditions at the NP surface. In our case, the usual continuity of the tangential components (\parallel) of the electric (\mathbf{E}) and magnetic (\mathbf{H}) field must be modified to account for the induced surface current, denoted here as \mathbf{K} , that arises from electrons in

the Dirac cone. The new boundary conditions read

$$(\mathbf{E}_{\parallel\text{out}} - \mathbf{E}_{\parallel\text{in}})_R = 0, \quad (3a)$$

$$(\mathbf{H}_{\parallel\text{out}} - \mathbf{H}_{\parallel\text{in}})_R = \mathbf{K}, \quad (3b)$$

through which we can extract the electric (a_ℓ) and magnetic (b_ℓ) Mie scattering coefficients [71], defined through $a_{E\ell m}^+ = a_\ell a_{E\ell m}^0$ and $a_{H\ell m}^+ = b_\ell a_{H\ell m}^0$, as

$$a_\ell = \frac{j_\ell(x_1)\Psi'_\ell(x_2)\varepsilon_1 - j_\ell(x_2)\Psi'_\ell(x_1)\varepsilon_2 + g(\omega, x_1)\Psi'_\ell(x_2)}{h_\ell^+(x_2)\Psi'_\ell(x_1)\varepsilon_2 - j_\ell(x_1)\xi'_\ell(x_2)\varepsilon_1 - g(\omega, x_1)\xi'_\ell(x_2)}, \quad (4a)$$

$$b_\ell = \frac{j_\ell(x_1)\Psi'_\ell(x_2)\mu_1 - j_\ell(x_2)\Psi'_\ell(x_1)\mu_2 + c(\omega, x_1)j_\ell(x_2)}{h_\ell^+(x_2)\Psi'_\ell(x_1)\mu_2 - j_\ell(x_1)\xi'_\ell(x_2)\mu_1 - c(\omega, x_1)h_{e\ell}^+(x_2)}, \quad (4b)$$

where $x_j = \frac{\omega}{c}\sqrt{\varepsilon_j\mu_j}R$ with c being the speed of light in vacuum, while ε_j and μ_j are the relative permittivity and permeability of the sphere ($j = 1$) and the host medium ($j = 2$), respectively. The corrections g and c are given by

$$g(\omega, x_1) = \frac{i\sigma\Psi'_\ell(x_1)}{\varepsilon_0\omega R}, \quad (5a)$$

$$c(\omega, x_1) = \frac{ix_0^2\sigma j_\ell(x_1)\mu_1\mu_2}{\varepsilon_0\omega R}, \quad (5b)$$

with the index 0 corresponding to vacuum. We assume that the permeabilities of all media are equal to unity. In addition, we introduced the Riccati-Bessel functions $\Psi_\ell(x) = xj_\ell(x)$ and $\xi_\ell(x) = xh_\ell^+(x)$, where j_ℓ and h_ℓ^+ are the spherical Bessel, and Hankel of first kind functions of order ℓ , respectively. The surface conductivity

$$\sigma = -\frac{i\omega\delta_R\varepsilon_0 R}{2}, \quad (6)$$

to which the surface current density \mathbf{K} corresponds, is obtained from the continuity equation $\nabla\mathbf{K} = -\frac{\partial\rho}{\partial t}$ at the NP surface, using the 2D divergence theorem, as the surface charge density $\rho = -a_{E\ell m}^{\text{in}}\delta_R\varepsilon_0$ resides precisely on the surface.

The scattering, extinction, and absorption cross sections, normalized to their geometric cross section πR^2 , can be expressed in terms of the Mie coefficients as

$$\begin{aligned} \sigma_{\text{sc}} &= \frac{2}{(kR)^2} \sum_{\ell} (2\ell + 1) (|a_\ell|^2 + |b_\ell|^2), \\ \sigma_{\text{ext}} &= -\frac{2}{(kR)^2} \sum_{\ell} (2\ell + 1) \text{Re}(a_\ell + b_\ell), \\ \sigma_{\text{abs}} &= \sigma_{\text{ext}} - \sigma_{\text{sc}}. \end{aligned} \quad (7)$$

Finally, experimental data are used for the dielectric function of Bi₂Se₃ [72], conveniently represented by a sum of three Lorentzians,

$$\varepsilon_1(\omega) = \sum_{i=\alpha,\beta,f} \frac{\omega_{\text{pi}}^2}{\omega_{\text{di}}^2 - \omega^2 - i\omega\gamma_i}, \quad (8)$$

plotted in Fig. 2(a). The subscripts i appearing in the sum in Eq. (8) stem from contributions of α and β phonons, as well as from bulk free-charge carriers f at low frequencies. The corresponding parameters for the three terms appearing in Eq. (8) are taken as $\hbar\omega_{p\alpha} = 79.4$ meV, $\hbar\omega_{p\beta} = 9.5$ meV, $\hbar\omega_{pf} = 47.6$ meV, $\hbar\omega_{0\alpha} = 8.3$ meV, $\hbar\omega_{0\beta} = 15.4$ meV, $\omega_{0f} = 0$ (by assumption), $\hbar\gamma_{\alpha} = 0.6$ meV, $\hbar\gamma_{\beta} = 0.3$ meV, and $\hbar\gamma_f = 1.0$ meV. We note that, since Bi_2Se_3 is anisotropic, we have assumed that the optical axis of the NP coincides with the direction of the wavevector of the incident EM wave, as illustrated in Fig. 1(b).

III. RESULTS AND DISCUSSION

In Figs. 2(b) and (c) we show extinction spectra in the absence of surface charges and currents, for two NP sizes, $R = 10$ nm and $R = 100$ nm, normalized to the geometric cross section πR^2 , decomposed into electric/magnetic (black/green lines) dipole (ED/MD: $\ell = 1$, solid lines), quadrupole (EQ/MQ: $\ell = 2$, dashed lines), and octupole (EO/MO: $\ell = 3$, dotted lines) contributions. It is evident that the ED contributions dominate the extinction spectrum in both cases, in accordance with the quasistatic approximation and previous studies of such NPs [43]. In addition, one can also see that MD modes related to the high permittivities due to the α and β phonons are, in principle, present, albeit three to five orders of magnitude weaker in these examples, and thus not contributing to the full spectrum; nevertheless, their existence can become important when the NP interacts with a QE, as we discuss later. At low energies, around 4 meV, a plasmonic mode emerges, originating from the f term of the dielectric function associated with free electrons within the bulk. These electrons arise from inevitable defects in the bulk [72]. Subsequently, at about 15 meV, a resonance originating from the β phonon coincides with the peak in the dielectric function [see inset in Fig. 2(a)], indicating excitation of the β bulk phonon polariton. At even higher energies, a surface phonon polariton (SPhP) becomes prominent, emerging exactly where $\text{Re}\epsilon_1 = -2$ [the Fröhlich condition for a resonance within the quasistatic approximation according to Eq. (6)—for $\delta_R = 0$]; the frequency at which this happens is indicated with a vertical dashed line in Fig. 2(a). This mode has already been proven responsible for a strong anisotropic Purcell effect in the case of microspheres [73–75]. For a 10 nm radius [Fig. 2(b)], the SPhP precisely aligns with the 66 meV mark of Fig. 2(a), while for larger radii [$R = 100$ nm in Fig. 2(c)], it only shifts slightly, to around 68 meV, due to retardation. In what follows, we will demonstrate that taking into account the surface states introduces DPPs, which lead to additional magnetic modes of topological nature, dramatically altering the optical response of the system.

TIs are theoretically anticipated to manifest robust conductivity on their surfaces, even in the presence of

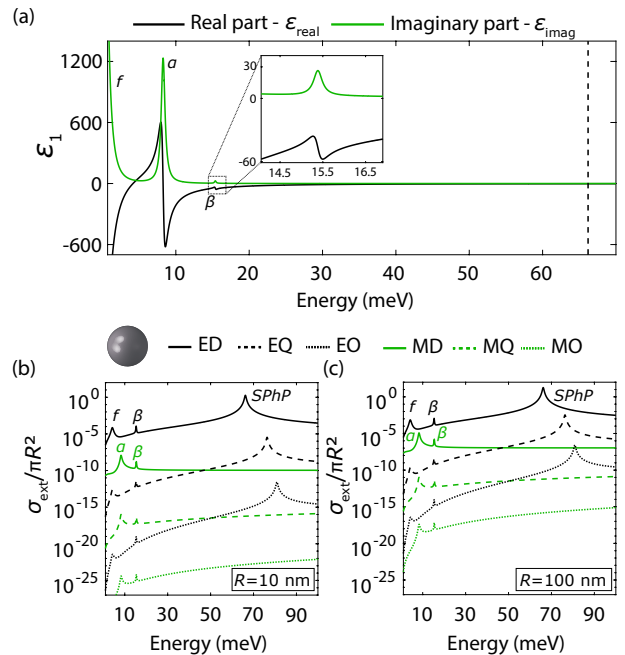


FIG. 2. (a) Real (black line) and imaginary part (green line) of the dielectric function of bulk Bi_2Se_3 [72] described by Eq. (8). The resonance around 8 meV corresponds to the α phonon, while the smaller resonance at about 15 meV (inset) corresponds to the β phonon. The vertical dashed line indicates the energy where $\text{Re}\epsilon_1 = -2$. (b, c) Contributions of dipolar (ED/MD, solid lines), quadrupolar (EQ/MQ, dashed lines), and octupolar (EO/MO, dotted lines) modes of both electric (in black) and magnetic (in green) character to the extinction cross section (log scale) of a Bi_2Se_3 nanosphere described by the dielectric function of (a), and radii (b) $R = 10$ nm and (c) $R = 100$ nm. The resonances related to free electrons (f), the α and β phonons, and the SPhP, are marked in each panel.

substantial impurities [76]; in principle, TIs are perfect conductors on their surfaces, potentially producing non-dissipative surface currents. However, it is necessary to take into account the coupling of the electrons in the Dirac cone with the bulk phonons, which have a pronounced presence in Bi_2Se_3 . Coupling of an electron with a phonon results in the destruction of the surface state and a topological phase change, i.e., the system transforms into a trivial insulator, and the generation of surface current is prevented. It should be emphasized that Bi_2Se_3 is a room-temperature TI, meaning that even at a temperature of 300 K, the Dirac cone persists, and the surface states are topologically protected. In spherical NPs, it has been found [43] that for radii larger than 37.5 nm the surface states may be disrupted due to interaction of electrons with phonons. This means that, in what follows, results for radii up to 37.5 nm can be considered valid at room temperature, while for larger sizes one should assume a temperature of 6 K.

For specific photon energies, the Bi_2Se_3 nanosphere, acting as a TI, undergoes transitions between surface

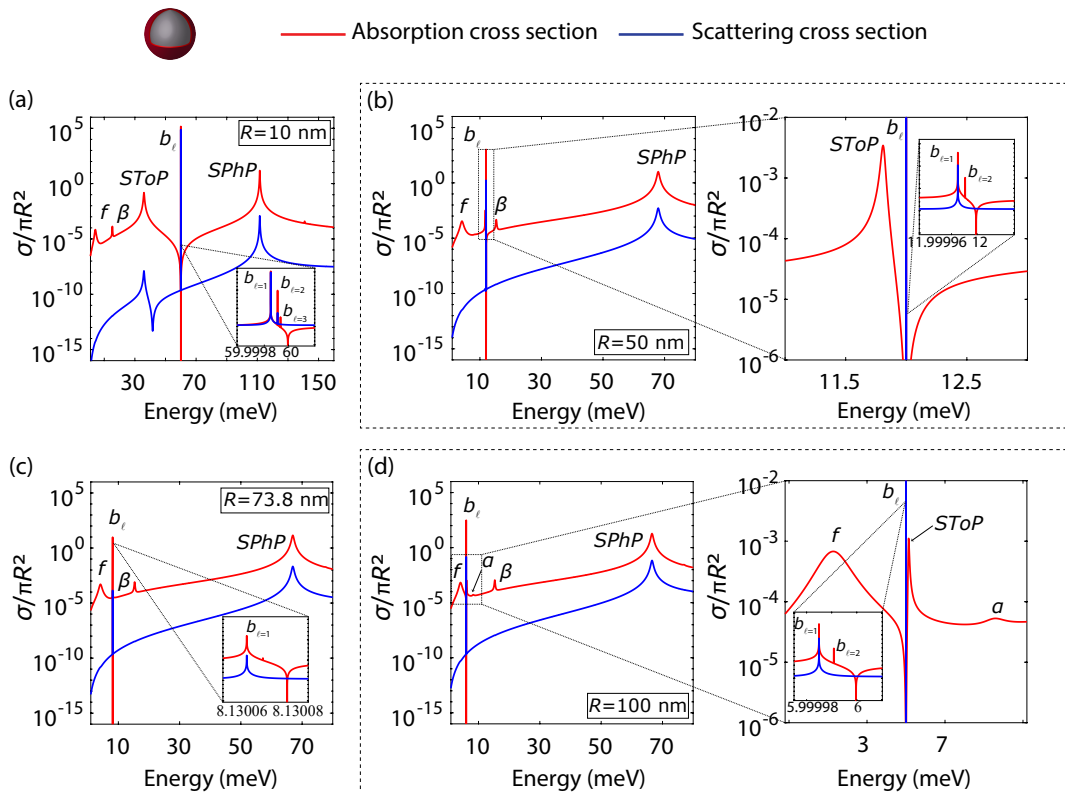


FIG. 3. Normalized absorption (red lines) and scattering (blue lines) cross sections (log scale) of Bi_2Se_3 nanospheres in which transitions between discrete levels at the surface states have been taken into account, for (a) $R = 10$ nm, (b) $R = 50$ nm, (c) $R = 73.8$ nm, and (d) $R = 100$ nm. In panels (a) and (c), the spectrum at the energy of the topological magnetic modes is depicted in the insets, and analyzed into multipolar contributions. In panel (a), the labels SToP and SphP characterize the hybrid modes emerging from the interaction of the two. In panel (c), the SToP mode is totally suppressed, as shown in Figure S3. In panels (b) and (d), the right-hand graphs are zooms into the frequency window of the SToP and induced magnetic modes, with their insets further focusing on just the magnetic multipoles.

states in the Dirac cone. In this work we consider transitions between the two lowest degenerate states, with energy $\mathcal{E} = -A/R$, and the two highest degenerate states, with energy $\mathcal{E} = A/R$, just below and above the Fermi energy $\mathcal{E}_F = 0$, which we take exactly at the Dirac point [see Fig. 1(a)]; this choice ensures an analytic expression for the surface charge density that can directly be implemented as a surface current in our calculations, while considering other transitions would require a more numerical—and thus less transparent—treatment. The response of the NP to an external electric field is predominantly influenced by the electrons near the Fermi level, and the most probable transition will occur between the aforementioned energy states. Importantly, the response of surface states varies according to the polarization of the incident radiation. This implies that a photocurrent will be generated precisely on the surface of the sphere. The exponential decay of surface states outside the surface region (which can be estimated as approximately 0.5 nm) [67] leads to the assumption that the topological surface current exists exactly at $r = R$.

Absorption and scattering spectra for $R = 10$ nm, 50 nm, 73.8 nm (which is a special value, as we discuss

below) and 100 nm are shown in Fig. 3, taking into account the surface states that give rise to a SToP mode, affected by coupling to the α phonon [for comparison with the quasistatic approximation, see also Fig. S.1(a)]. It is established that interaction between the modes sustained by opposite surfaces can occur, resulting in the formation of a gap in the Dirac cone. Experiments have shown that, in the case of Bi_2Se_3 , a film thickness of less than six quintuple layers is the limit at which a finite energy gap appears [77]. For this reason, the smallest radius examined below is set at 10 nm. On the other hand, the radius of 100 nm represents the maximum size that the nanosphere can attain before transitioning to a nearly-continuum of surface states, with energy differences outside our frequency window. The SToP mode, resulting from the interaction of Dirac electrons with the α phonon, is depicted in Fig. 3(a) at about 36 meV (this is, in fact, a special case analyzed in more detail in Fig. 4), in Fig. 3(b) at about 12 meV, and in (d) at about 6 meV, and is of ED character ($a_{\ell=1}$). For $R = 73.8$ nm [Fig. 3(c)], the SToP mode disappears (see Fig. S.2), as it is entirely absorbed by the α phonon [78]. In addition to these findings of previous studies, our fully electrody-

dynamic calculations further reveal—apart from the weak bulk magnetic modes mentioned previously—the emergence of magnetic *topological* modes, denoted as b_ℓ , manifesting as needle-like peaks in the zoomed graphs; interestingly, these modes do survive for $R = 73.8$ nm. We also demonstrate the possibility of magnetic Mie modes stemming from the bulk phonons (see Figure S2) which can contribute to the extinction cross sections in the case of large nanospheres, such as 100 nm, as can be seen in Fig. 3(d) (α phonon). The magnetic topological modes arise from the current at the surface of the TI. Notably, a zero-absorption point can be observed for every radius, where the electric field inside the NP tends to zero. This implies that in this energy region the NP transforms into a perfect conductor, allowing for the presence of surface currents originating from the surface charge density generated from transitions between the discrete levels in the Dirac cone with energy difference $\Delta\mathcal{E}$.

We also observe that by reducing the radius, the topological modes are enhanced, and their linewidths are modified. As the NP decreases in size, the ratio of bulk material to surface diminishes, resulting in increased prominence of surface states. It is still clear that in each case a point of zero absorption is detected, where the electric field inside the NP is zero, and the nanosphere transforms into a perfect conductor. Fig. 3(d) shows that these topological optical modes are essentially Fano resonances [79], as they have a narrow and asymmetric lineshape. Specifically, in the case of the SToP mode, the discrete surface state excitation corresponds to the resonant process, while the coupling with the phonon mode, which is broader in comparison, corresponds to the background process. On the other hand, there is no interaction of the magnetic modes b_ℓ with a background process, resulting in the appearance of extremely sharp resonances, with the linewidth again related to the absence of an imaginary part in Eq. (1). The multipolar analysis of the spectra is further extended in Fig. S.3, wherein a detailed representation of the contributions from all multipoles in the $R = 100$ nm NP is depicted.

To shed more light on the influence of surface states on the spectra, we examine various NP radii, which adjust the energy at which the surface charge density emerges, as it depends on the factor $2A/R$. In Fig. 4, it becomes evident that the surface states induce a shift of the polaritonic modes, implying a splitting of the modes. The radii in the figure are chosen in such a way that the surface states coincide with similar resonant frequencies of the modes of the trivial-insulator NP. In the case of $R = 37.5$ nm [Figs. 4(a) and (b)], when the surface states are excited in the frequency region of the β phonon, a splitting of the bulk phonon polariton mode occurs in absorption, as can be seen in the inset of Fig. 4(b). However, this splitting is not pronounced, as it involves interactions between the bulk optical mode and the surface optical mode. On the other hand, in the case of $R = 10$ nm we observe a very strong splitting of the SPhP mode, in both scattering and absorption, revealing a new

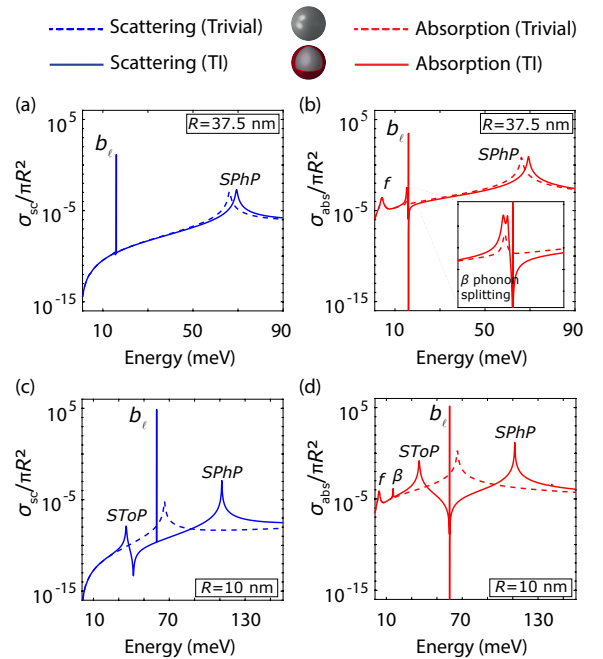


FIG. 4. (a) Normalized scattering and (b) absorption cross section for a trivial-insulator (dashed lines) and a TI (solid lines) Bi_2Se_3 nanosphere, (i.e., without and with surface states) for $R = 37.5$ nm. Splitting of the β bulk phonon polariton is shown in the zoom-in inset of (b). (c), (d) Same as (a), (b), for $R = 10$ nm. In this case, splitting of the SPhP is observed in both scattering and absorption. The labels SToP and SPhP refer to the lower- and higher-energy hybrid modes that emerge from the interaction of the individual SToP and SPhP.

situation of self-hybridization between different states of the same system [80, 81], as illustrated in Figs. 4(c) and (d) at 36 meV. This response can be interpreted as follows: the topological surface current results in blocking the emergence of the SPhP, shifting it to side frequencies where the current vanishes. This is clearly visible by Figs. 4(c) and (d) featuring the distinct magnetic topological mode between resonances with a mixed SToP and SPhP character.

Based on the Fano shape that characterizes the new topological modes, we expect that the rate of excitation of QEs that have intrinsic magnetic transitions in the region of THz, such as erbium ions (Er^{3+}) [82], can be drastically modified. The interaction of TI NPs with QEs with electric transitions has been investigated within the quasistatic regime, revealing the presence of high electric PFs [83]. In view of our discussion above, we now explore the complete EM solution for the interaction of QEs with a Bi_2Se_3 nanosphere, taking into consideration all the aforementioned phenomena (topological surface current, magnetic modes, surface mode splitting). Because of the presence of magnetic modes, we also consider magnetic dipoles, whose transitions are typically many orders of magnitude slower. The electric (E) and magnetic (M)

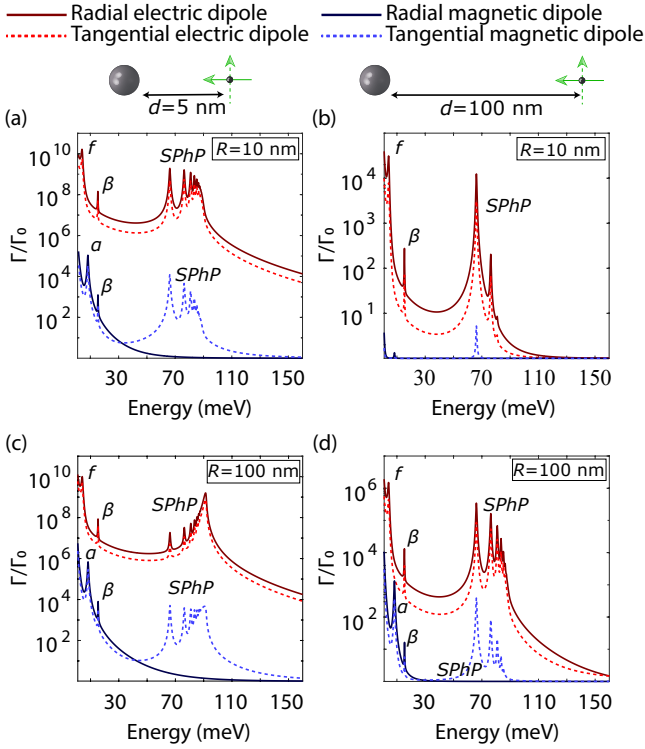


FIG. 5. PFs (log scale) for a QE with electric (red line) or magnetic (blue line) dipole transitions, radially (solid lines) or tangentially (dashed lines) oriented with respect to the surface of a Bi_2Se_3 nanosphere of radius R , as shown in the schematics, in the absence of surface states. (a) The QE is placed at a distance of $d = 5$ nm, and $R = 10$ nm; (b) $d = 100$ nm, and $R = 10$ nm; (c) $d = 5$ nm, and $R = 100$ nm; (d) $d = 100$ nm, and $R = 100$ nm.

PFs are calculated by the following relations [17]

$$\frac{\Gamma_E^\perp}{\Gamma_0} = 1 - \frac{3}{2} \text{Re} \sum_{\ell=1}^{\infty} (2\ell + 1)\ell(\ell + 1)a_\ell \left[\frac{h_\ell^+(x_2)}{x_2} \right]^2 \quad (9a)$$

$$\frac{\Gamma_E^\parallel}{\Gamma_0} = 1 - \frac{3}{4} (2\ell + 1) \text{Re} \sum_{\ell=1}^{\infty} \left\{ a_\ell \left[\frac{\xi_\ell(x_2)}{x_2} \right]^2 + b_\ell h_\ell^{+2}(x_2) \right\} \quad (9b)$$

$$\frac{\Gamma_M^\perp}{\Gamma_0} = 1 - \frac{3}{2} \text{Re} \sum_{\ell=1}^{\infty} (2\ell + 1)\ell(\ell + 1)b_\ell \left[\frac{h_\ell^+(x_2)}{x_2} \right]^2 \quad (9c)$$

$$\frac{\Gamma_M^\parallel}{\Gamma_0} = 1 - \frac{3}{4} (2\ell + 1) \text{Re} \sum_{\ell=1}^{\infty} \left\{ b_\ell \left[\frac{\xi_\ell(x_2)}{x_2} \right]^2 + a_\ell h_\ell^{+2}(x_2) \right\}, \quad (9d)$$

where the decay rate of an electric (magnetic) dipole in the case of a radial and tangential orientation, relatively to the NP surface (see sketches in Fig. 5), is denoted as Γ_E^\perp (Γ_M^\perp), and Γ_E^\parallel (Γ_M^\parallel), respectively. The decay rate in vacuum is denoted as Γ_0 .

To highlight the extent of the changes that an electrodynamic description can bring to the QE–NP inter-

action, we first calculate in Fig. 5 the PFs for a Bi_2Se_3 nanosphere *without* surface states, considering cases with radii of 10 nm and 100 nm, at QE-to-NP surface distances of $d = 5$ nm and $d = 100$ nm. Both near and far from the NP surface, significantly enhanced spontaneous emission rates are observed, as a result of the strong interaction between the QE and the NP eigenmodes. Specifically, for the electric-dipole case, resonances occur for frequencies corresponding to the plasmonic mode f , the β bulk phonon polariton mode, and the SPhP. Notably, these resonances do not shift in energy by varying the NP size or the emitter distance, but they do change in linewidth. Within the resonance region of the SPhP (70 – 100 eV), additional peaks emerge due to the higher-order multipolar SPhPs, which do not manifest in the extinction spectra, but their existence was demonstrated in Figs. 2(b) and (c). Concerning the magnetic dipole case, resonances linked to both the α bulk phonon polariton at about 8 meV and the β bulk phonon polariton at 15 meV emerge, aligning with the corresponding resonances of the dielectric function. Similarly, coupling occurs with the SPhPs, albeit only when the dipole is oriented parallel to the NP surface, showcasing coupling with analogous higher-order multipolar modes. Our calculations show that the first SPhP mode is the main contributor to the radiative enhancement of the Purcell effect, while the other resonances correspond to nonradiative decay. It is remarkable that the PF values for a magnetic dipole interacting with the bulk α phonon mode are of the order of 10^6 , while they still reach values of 10^4 when interacting with the other modes. The reason for such a strong light–matter interaction of magnetic nature lies in the fact that the high-refractive-index dielectric generates displacement current loops, inducing magnetic resonances.

Extending our investigation, we provide in Fig. 6 the corresponding PFs when surface states are included [for a comparison with the quasistatic approach, see Fig. S.1(b)], and analyze further the influence of DPPs on the QE–NP coupling. The impact of surface states dramatically alters the spectrum, as expected for surface polaritons. The resilience of the plasmonic f mode and the β bulk phonon polariton is still obvious, but the impact of surface states becomes more evident in the enhanced PF values observed at the frequencies of the DPPs. Specifically, DPPs couple efficiently with the electric dipole, leading to pronounced SToP-related PF enhancement, while their coupling with the magnetic dipole leads to PF enhancement due to the topological magnetic modes (b_l), manifesting as the needle-like resonances shown in the insets. Comparing with Fig. 5, shifting of the resonances of the spontaneous emission rate is also noticeable, as the SPhP splitting emerges for $R = 10$ nm. Furthermore, in the case where the QE is positioned at a distance of 5 nm [Figs. 6(a) and (c)], the Purcell enhancement factors exhibit a colossal increase, while, at the same time, the emitter couples with many higher-order multipolar modes. These results imply that

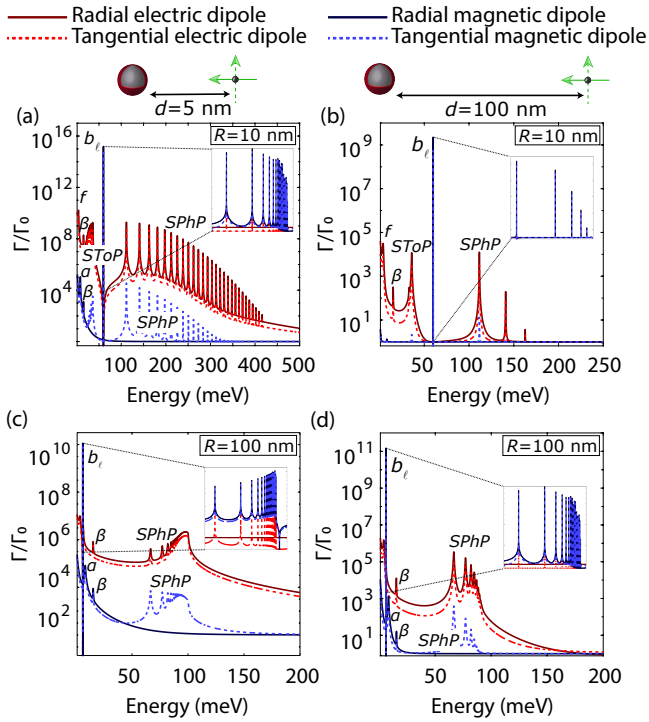


FIG. 6. Same as Fig. 5, but with surface-states taken into account. The insets zoom in at the energies of the b_ℓ resonances.

the QE interacts strongly with the conducting surface of the nanosphere, specifically with the surface charge density which is coupled with the SPhP, giving rise to DPPs. The strong interaction arising from intense oscillations of the induced surface current is confirmed by the zoomed-in frequency regions surrounding the induced magnetic eigenmodes. It is also noteworthy that these high PFs survive even at significant distances from the NP surfaces, as shown in Figs. 6(b) and (d).

The interaction of an electric-dipole QE with the DPP excited at the surface of the TI results in a finite PF, as expected. The mechanism that prevents higher values is the phonon-induced damping rate introduced into the dielectric function. However, the interaction of magnetic-dipole QEs with the b_ℓ magnetic modes yields unphysically high magnetic PFs. As we mentioned earlier, the origin of delta-like resonances in either extinction or PF can be attributed to the absence of a finite lifetime for the surface states in Eq. (1). To address this issue, we introduce in Fig. 7 damping rates for the surface states by hand, to account for the finite lifetimes of the excited Dirac electrons. More specifically, we introduce an imaginary term $i\Gamma$ into the denominators of Eq. (1), which is now modified to

$$\delta_R(\omega) = \frac{e^2}{6\pi\epsilon_0 R} \left(\frac{1}{2\Delta\mathcal{E} - \hbar\omega - i\Gamma} + \frac{1}{2\Delta\mathcal{E} + \hbar\omega - i\Gamma} \right). \quad (10)$$

In this expression, we use for Γ two different values based on the lifetimes of DPPs [84–87], although we anticipate that these values, which correspond to calculations or measurements of surface states in large systems and with several co-acting damping mechanisms, might heavily underestimate the lifetime of the transitions between quantized surface states. It is also worth keeping in mind that, since the transitions under study only concern one or two surface electrons per Brillouin zone, the corresponding recombination channels are rather limited, and the excited states are expected to be quite long-lived. Focusing on a sphere with $R = 10$ nm, we initially incorporate a $\Gamma = 0.1$ THz, corresponding to lifetime $\tau = 10$ ps; subsequently we shift to a—possibly extreme— $\Gamma = 1$ THz, corresponding to $\tau = 1$ ps. For both lifetimes, the extinction cross sections in Figs. 7(a) and (b) demonstrate that both the topological electric mode and the resonance splitting due to the interaction of the SPhP and the DPP persist. We thus conclude from Fig. 7(b) that, even for high damping rates of the excited surface states, the NP sustains its topological optical modes. We calculated similar broadening, with the main resonances still surviving, for an intermediate radius $R = 50$ nm, plotted in Fig. S.4.

Subsequently, we calculate in Figs. 7(c) and (d) the corresponding PFs, for a QE positioned at distance $d = 5$ nm from the NP surface. Interestingly, we observe comparable resonances and footprints as in the infinite-lifetime case. As expected, the topological magnetic Purcell enhancement now attains a finite—yet significantly high—value of $\sim 10^4$, while the topological electric PF assumes values of $\sim 2.0 \times 10^8$. For larger spheres, such as $R = 50$ nm at QE-to-NP surface distances of $d = 5$ nm, the magnetic (electric) PF originating from the excitation of DPPs is still considerable, as high as $\sim 1.0 \times 10^5$ ($\sim 3.0 \times 10^8$) considering the same lifetimes as in Figs. 7(c) and (d) (see Fig. S.4). The PFs are higher for this larger-dimension case, because the topological surface currents circulate on a larger NP surface. These results suggest that even for large damping rates, the TI NP still manifests magnetic modes due to the existence of DPPs.

IV. CONCLUSIONS

We employed fully electrodynamic analytical calculations based on Mie theory, to demonstrate the emergence of topological magnetic modes resulting from the interaction of THz radiation with Bi_2Se_3 spherical TIs. In particular, we observed the excitation of previously unreported magnetic modes, induced by topological surface currents that are related to transitions between discrete energy levels in the Dirac cone, generating currents along the conductive surface of the NPs. For specific NP sizes, these topological surface currents can even lead to striking mode splitting in absorption and scattering spectra, as a result of the self-hybridization between DPPs and SPhPs. These modes, distinguished by their Fano-like shape, produce robust coupling effects over a wide win-

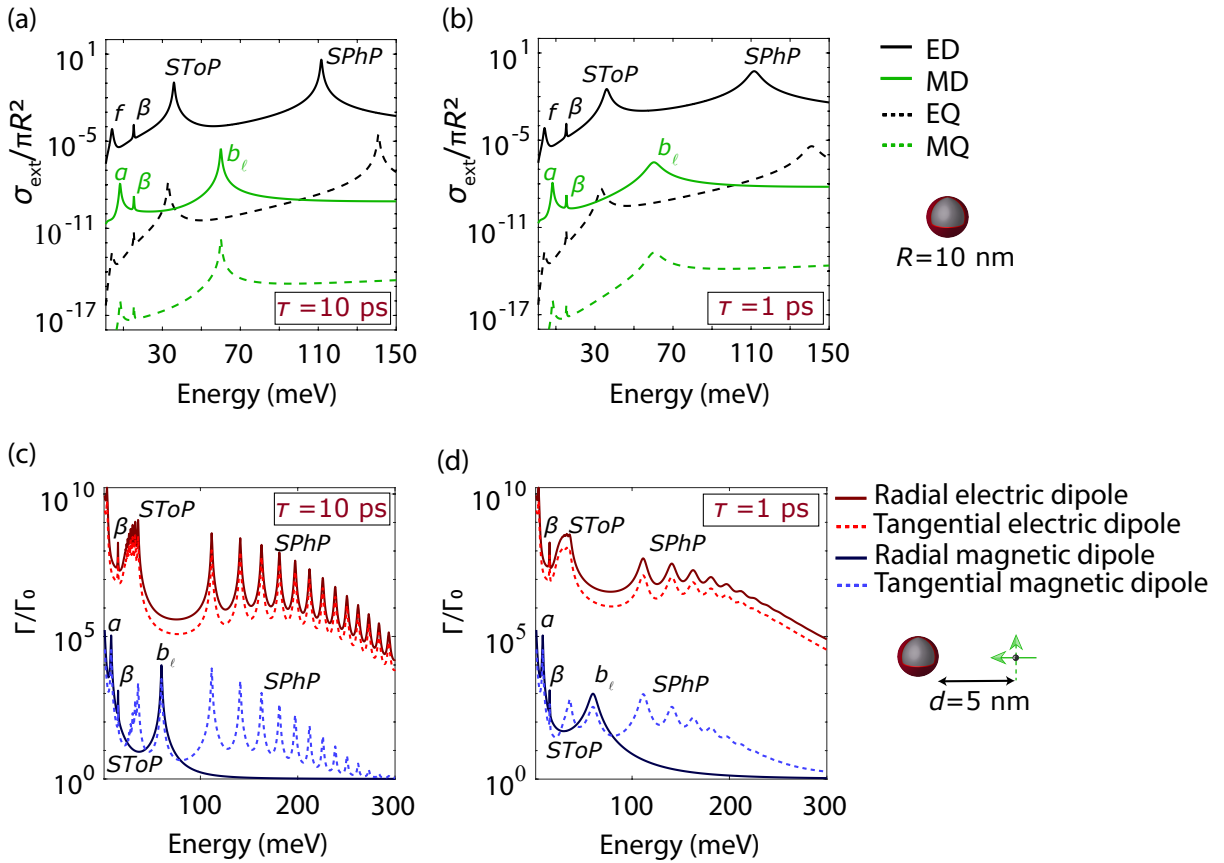


FIG. 7. (a) Decomposition of the normalized extinction cross section of a Bi_2Se_3 nanosphere of radius $R = 10$ nm into ED (solid black line), EQ (dashed black line), MD (solid green line), and MQ (dashed green line) contributions, considering a damping mechanism with $\tau = 10$ ps. (b) Same as (a), for $\tau = 1$ ps. (c) PFs of electric- (red lines) or magnetic-dipole (blue lines) transitions, radially (solid lines) and tangentially (dashed lines) oriented to the NP surface, for the NP of (a, b), at QE–NP distance $d = 5$ nm, and $\tau = 10$ ps. (d) Same as (c), for $\tau = 1$ ps.

dow of energies, for QEs at a broad range of distances from the NP. Additionally, we identified strong light–matter interaction of magnetic nature, since the high-refractive-index dielectric generates displacement current loops in the bulk, stimulating substantial Mie-type magnetic response. As a result, we calculated remarkable magnetic and electric Purcell enhancement over a wide energy window from a few THz to a few hundreds of THz. This response arises from the synergy between topological surface plasmons and bulk NP modes. The magnetic PFs obtained through the coupling of QEs with bulk phonon polaritons are notably high, reaching values of up to $\sim 7 \times 10^5$. Simultaneously, the magnetic PFs associated with DPPs remain significantly large ($\sim 10^4$ to 10^5) even when realistic lifetimes for the surface states are considered. Bi_2Se_3 nanospheres demonstrate thus a rich optical response that pertains to both the bulk and the topologically protected surface states, enabling the excitation of DPPs, and are positioned as promising candidates for facilitating strong light–matter interactions in nanophotonics and quantum optics. Our results have the potential to trigger further research for QEs with mag-

netic transitions in the THz, or for the acceleration of otherwise forbidden atomic transitions.

ACKNOWLEDGMENTS

N. A. M. is a VILLUM Investigator supported by VILLUM Fonden (grant No. 16498). The Center for Polariton-driven Light–Matter Interactions (POLIMA) is sponsored by the Danish National Research Foundation (Project No. DNRF165).

Appendix A: Full EM calculations vs quasistatic regime

In order to elucidate the significance of the full electromagnetic solution, which includes all multipolar contributions (solid lines), and to emphasize the difference from the quasistatic approximation, i.e., only the electric dipole modes (dashed lines), we provide Fig. S.1. It should be further noted that the solid lines, associated with Mie resonances and the new topological magnetic modes, are not discernible with the quasistatic approximation.

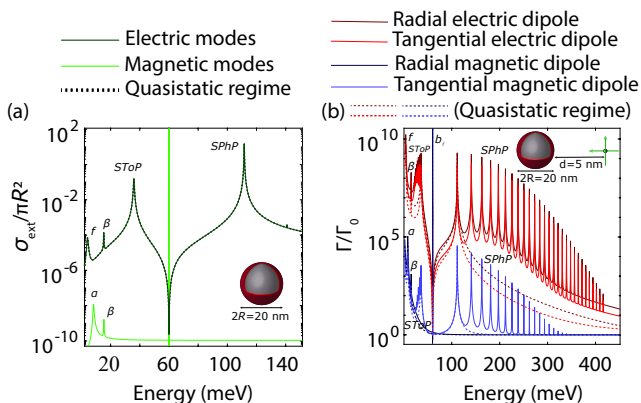


FIG. S.1. (a) Normalized extinction cross section (log scale) of a Bi_2Se_3 nanosphere of radius $R = 10$ nm in the cases of the quasistatic approach (dashed lines) and in the case of the full electrodynamic solution (solid lines). (b) Purcell factors (log scale) with electric (red line) or magnetic (blue line) dipole transitions, radially (dark color) and tangentially (light color) oriented to the NP surface, with radius same as (a) and emitter–nanoparticle distance $d = 5$ nm, for the quasistatic regime (dashed lines) and for all contributions from the multipolar expansion (solid lines).

Appendix B: Extinction of the STOP mode

In Fig. S.2, we present the optical response of a Bi_2Se_3 nanosphere with a radius of $R = 73.8$ nm, focusing on the energy region where the excitation of surface states occurs, aiming to distinguish between the modes. The specific value for the radius represents the unique condition at which the surface topological optical (SToP) mode disappears. Nevertheless, the induced magnetic modes b_l remain, as indicated by the graph.

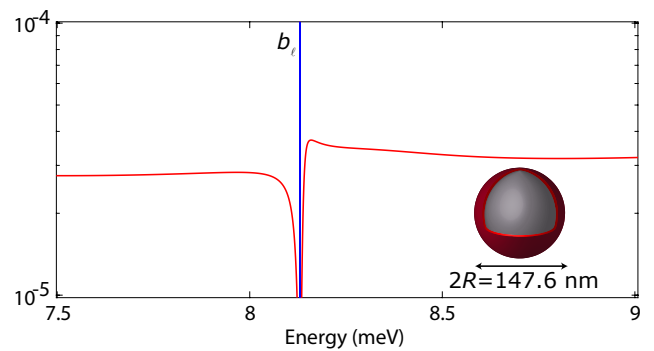


FIG. S.2. Normalized absorption (red lines) and scattering (blue lines) cross sections (log scale) of a Bi_2Se_3 nanosphere in which transitions between discrete levels at the surface states have been taken into account, for $R = 73.8$ nm.

Appendix C: Multipolar decomposition

We extend the analysis of the optical response of a spherical topological insulator in Fig. S.3, wherein a detailed representation of the contributions from the multipolar expansion, for a nanosphere with a radius of $R = 100$ nm is depicted.

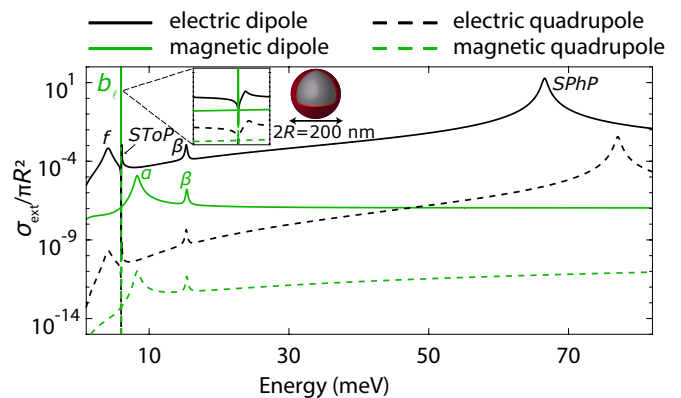


FIG. S.3. Multipolar decomposition via Mie coefficients of electric dipolar (black solid line), magnetic dipolar (dashed black line), electric quadrupolar (green line), and magnetic quadrupolar (dashed green line) contributions to the normalized extinction cross section (log scale) for a spherical topological insulator with $R = 100$ nm.

Appendix D: Role of damping

For confirmation of the persistence of Dirac plasmon polaritons when introducing a limited lifetime of excited states, we study in Fig. S.4 a nanoparticle with radius $R = 50$ nm. The multipolar decomposition of the extinction cross section is shown in Figs. S.4(a) and (b), while the corresponding Purcell factors are plotted in Figs. S.4(c) and (d), for emitter–nanoparticle distance of $d = 5$ nm. We explore two different lifetimes, $\tau = 1$ ps and $\tau = 10$ ps.

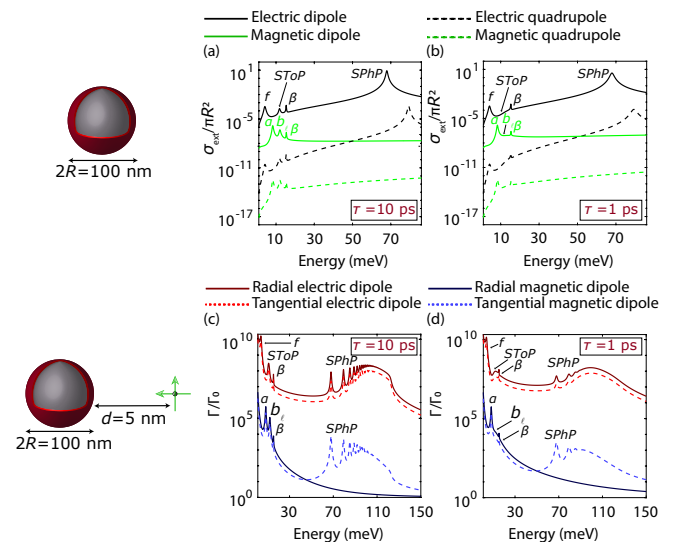


FIG. S.4. (a, b) Decomposition of the normalized extinction cross section (log scale) of a Bi_2Se_3 nanosphere of radius $R = 50$ nm into electric dipolar (solid black line), electric quadrupolar (dashed black line), magnetic dipolar (solid green line), and magnetic quadrupolar (dashed green line) contributions, considering a damping mechanism with (a) $\tau = 10$ ps and (b) $\tau = 1$ ps. (c, d) Purcell factors with electric- (red line) or magnetic-dipole (blue line) transitions, radially (dark color) and tangentially (light color) oriented to the nanoparticle surface, with radius same as in (a, b), emitter–nanoparticle distance $d = 5$ nm, and (c) $\tau = 10$ ps or (d) $\tau = 1$ ps.

* niky@mci.sdu.dk

† ct@mci.sdu.dk

- [1] F. Bernardot, P. Nussenzevig, M. Brune, J. M. Raimond, and S. Haroche, *Europhys. Lett.* **17**, 33 (1992).
- [2] P. Törmä and W. L. Barnes, *Rep. Prog. Phys.* **78**, 013901 (2015).
- [3] C. Tserkezis, A. I. Fernández-Domínguez, P. A. D. Gonçalves, F. Todisco, J. D. Cox, K. Busch, N. Stenger, S. I. Bozhevolnyi, N. A. Mortensen, and C. Wolff, *Rep. Prog. Phys.* **83**, 082401 (2020).
- [4] N. T. Fofang, T.-H. Park, O. Neumann, N. A. Mirin, P. Nordlander, and N. J. Halas, *Nano Lett.* **8**, 3481 (2008).
- [5] G. Zengin, M. Wersäll, S. Nilsson, T. J. Antosiewicz, M. Käll, and T. Shegai, *Phys. Rev. Lett.* **114**, 157401 (2015).
- [6] P. A. D. Gonçalves, T. Christensen, N. Rivera, A.-P. Jauho, N. A. Mortensen, and M. Soljačić, *Nat. Commun.* **11**, 366 (2020).
- [7] A. Cuartero-González and A. I. Fernández-Domínguez, *ACS Photonics* **5**, 3415 (2018).
- [8] M. Kupresak, X. Zheng, R. Mittra, G. A. E. Vandenbosch, and V. V. Moshchalkov, *Nanoscale Adv.* **4**, 2346 (2022).
- [9] J. Yuen-Zhou, W. Xiong, and T. Shegai, *J. Chem. Phys.* **156**, 030401 (2022).
- [10] S. V. Boriskina, T. A. Cooper, L. Zeng, G. Ni, J. K. Tong, Y. Tsurimaki, Y. Huang, L. Meroueh, G. Mahan, and G. Chen, *Adv. Opt. Phot.* **9**, 775 (2017).
- [11] J. B. Khurgin, *Nat. Nanotechnol.* **10**, 2 (2015).
- [12] D. G. Baranov, R. S. Savelev, S. V. Li, A. E. Krasnok, and A. Alù, *Laser Phot. Rev.* **11**, 1600268 (2017).
- [13] C. Tserkezis, P. A. D. Gonçalves, C. Wolff, F. Todisco, K. Busch, and N. A. Mortensen, *Phys. Rev. B* **98**, 155439 (2018).
- [14] A. García-Etxarri, R. Gómez-Medina, L. S. Froufe-Pérez, C. López, L. Chantada, F. Scheffold, J. Aizpurua, M. Nieto-Vesperinas, and J. J. Sáenz, *Opt. Express* **1**, 4815 (2011).
- [15] A. B. Evlyukhin, S. M. Novikov, U. Zywietz, R. L. Erikssen, C. Reinhardt, S. I. Bozhevolnyi, and B. N. Chichkov, *Nano Lett.* **12**, 3749 (2012).
- [16] P. E. Stamatopoulou and C. Tserkezis, *OSA Cont.* **4**, 918 (2021).
- [17] M. K. Schmidt, R. Esteban, J. J. Sáenz, I. Suárez-Lacalle, S. Mackowski, and J. Aizpurua, *Opt. Express* **20**, 13636 (2012).
- [18] Y. Brûlé, P. Wiecha, A. Cuche, V. Paillard, and G. Colas des Francs, *Opt. Express* **30**, 20360 (2022).
- [19] E. M. Purcell, *Phys. Rev.* **69**, 681 (1946).
- [20] J. Sloan, N. Rivera, J. D. Joannopoulos, I. Kaminer, and M. Soljačić, *Phys. Rev. B* **100**, 235453 (2019).
- [21] J. Moore, *Nature* **464**, 194 (2010).

- [22] A. Kitaev and J. Preskill, *Phys. Rev. Lett.* **96**, 110404 (2006).
- [23] X.-L. Qi, H. Katsura, and A. W. W. Ludwig, *Phys. Rev. Lett.* **108**, 196402 (2012).
- [24] K. Tschernig, A. Jimenez-Galán, D. N. Christodoulides, M. Ivanov, K. Busch, M. A. Bandres, and A. Perez-Leija, *Nat. Commun.* **12**, 1974 (2021).
- [25] L. Lu, J. D. Joannopoulos, and M. Soljačić, *Nat. Photon.* **8**, 821 (2014).
- [26] N. A. Mortensen, S. I. Bozhevolnyi, and A. Alù, *Nanophotonics* **8**, 1315 (2019).
- [27] M. S. Rider, A. Buendía, D. R. Abujetas, P. A. Huidobro, J. A. Sánchez-Gil, and V. Giannini, *ACS Photonics* **9**, 1483 (2022).
- [28] M. Hafezi, S. Mittal, J. Fan, A. Migdall, and J. M. Taylor, *Nat. Photon.* **7**, 1001 (2013).
- [29] S. Barik, A. Karasahin, C. Flower, T. Cai, H. Miyake, W. DeGottardi, M. Hafezi, and E. Waks, *Science* **359**, 666 (2018).
- [30] V. Yannopapas, *Phys. Rev. B* **84**, 195126 (2011).
- [31] T. Christensen, H. C. Po, J. D. Joannopoulos, and M. Soljačić, *Phys. Rev. X* **12**, 021066 (2022).
- [32] G.-J. Tang, X.-T. He, F.-L. Shi, J.-W. Liu, X.-D. Chen, and J.-W. Dong, *Laser Phot. Rev.* **16**, 2100300 (2022).
- [33] Z. Wang, Y. Chong, J. D. Joannopoulos, and M. Soljačić, *Nature* **461**, 772 (2009).
- [34] A. Khanikaev, S. Mousavi, W.-K. Tse, M. Kargarian, A. H. MacDonald, and G. Shvets, *Nat. Mater.* **12**, 233 (2013).
- [35] C. A. Rosiek, G. Arregui Bravo, A. Vladimirova, M. Albrechtsen, B. V. Lahijani, R. E. Christiansen, and S. Stobbe, *Nat. Photon.* **17**, 386 (2023).
- [36] P. Di Pietro, M. Ortolani, O. Limaj, A. Di Gaspare, V. Giliberti, F. Giorgianni, M. Brahlek, N. Bansal, N. Koirala, S. Oh, P. Calvani, and S. Lupi, *Nat. Nanotechnol.* **8**, 556 (2013).
- [37] T. P. Ginley and S. Law, *Adv. Opt. Mater.* **6**, 1800113 (2018).
- [38] P. Di Pietro, N. Adhlakha, F. Piccirilli, A. Di Gaspare, J. Moon, S. Oh, S. Di Mitri, S. Spampinati, A. Perucchi, and S. Lupi, *Phys. Rev. Lett.* **124**, 226403 (2020).
- [39] S. Chen, A. Bylinkin, Z. Wang, M. Schnell, G. Chandan, P. Li, A. Nikitin, S. Law, and R. Hillenbrand, *Nat. Commun.* **13**, 1374 (2022).
- [40] T. Ginley, Y. Wang, Z. Wang, and S. Law, *MRS Commun.* **8**, 782 (2018).
- [41] F. D. M. Haldane, *Phys. Rev. Lett.* **61**, 2015 (1988).
- [42] K.-I. Imura, Y. Yoshimura, Y. Takane, and T. Fukui, *Phys. Rev. B* **86**, 235119 (2012).
- [43] G. Siroki, D. K. K. Lee, P. D. Haynes, and V. Giannini, *Nat. Commun.* **7**, 12375 (2016).
- [44] M. S. Rider, M. Sokolikova, S. M. Hanham, M. Navarro-Cía, P. D. Haynes, D. K. K. Lee, M. Daniele, M. Cestelli Guidi, C. Mattevi, S. Lupi, and V. Giannini, *Nanoscale* **12**, 22817 (2020).
- [45] I. Staude, A. E. Miroschnichenko, M. Decker, N. T. Fofang, S. Liu, E. Gonzales, J. Dominguez, T. S. Luk, D. N. Neshev, I. Brener, and Y. Kivshar, *ACS Nano* **7**, 7824 (2013).
- [46] Y. Kivshar, *Nano Lett.* **22**, 3513 (2022).
- [47] N. Rivera, I. Kaminer, B. Zhen, J. D. Joannopoulos, and M. Soljačić, *Science* **353**, 263 (2016).
- [48] M. Zhang, H. Y. Jia, J. S. Huang, and L. F. Wei, *Opt. Lett.* **35**, 1686 (2010).
- [49] E. Forati, G. W. Hanson, and S. Hughes, *Phys. Rev. B* **90**, 085414 (2014).
- [50] M. Z. Hasan and C. L. Kane, *Rev. Mod. Phys.* **82**, 3045 (2010).
- [51] C. L. Kane and E. J. Mele, *Phys. Rev. Lett.* **95**, 226801 (2005).
- [52] D. Jin, T. Christensen, M. Soljačić, N. X. Fang, L. Lu, and X. Zhang, *Phys. Rev. Lett.* **118**, 245301 (2017).
- [53] T. G. Rappoport, Y. V. Bludov, F. H. L. Koppens, and N. M. R. Peres, *ACS Photonics* **8**, 1817 (2021).
- [54] J. E. Moore and L. Balents, *Phys. Rev. B* **75**, 121306 (2007).
- [55] C. Kastl, C. Kärnetzky, H. Karl, and A. Holleitner, *Nat. Commun.* **6**, 6617 (2015).
- [56] L. Luo, X. Yang, X. Liu, Z. Liu, C. Vaswani, D. Cheng, M. Mootz, X. Zhao, Y. Yao, C.-Z. Wang, K.-M. Ho, I. E. Perakis, M. Dobrowolska, J. K. Furdyna, and J. Wang, *Nat. Commun.* **10**, 607 (2019).
- [57] L. Fu, C. L. Kane, and E. J. Mele, *Phys. Rev. Lett.* **98**, 106803 (2007).
- [58] M. Z. Hasan and J. E. Moore, *Ann. Rev. Condens. Matter Phys.* **2**, 55 (2011).
- [59] C. L. Kane and E. J. Mele, *Phys. Rev. Lett.* **95**, 146802 (2005).
- [60] H. Zhang, C.-X. Liu, X.-L. Qi, X. Dai, Z. Fang, and S.-C. Zhang, *Nat. Phys.* **5**, 438 (2009).
- [61] K.-I. Imura, Y. Takane, and A. Tanaka, *Phys. Rev. B* **84**, 195406 (2011).
- [62] X. Zhang, J. Wang, and S.-C. Zhang, *Phys. Rev. B* **82**, 245107 (2010).
- [63] W. Tang, A. Politano, C. Guo, W. Guo, C. Liu, L. Wang, X. Chen, and W. Lu, *Adv. Funct. Mater.* **28**, 1801786 (2018).
- [64] D. Pesin and A. H. MacDonald, *Nat. Mater.* **11**, 409 (2012).
- [65] H.-H. Kung, S. Maiti, X. Wang, S.-W. Cheong, D. L. Maslov, and G. Blumberg, *Phys. Rev. Lett.* **119**, 136802 (2017).
- [66] R. Salikhov, I. Ilyakov, L. Körber, A. Kákay, R. Gallardo, A. Ponomaryov, J.-C. Deinert, T. Oliveira, K. Lenz, J. Fassbender, S. Bonetti, O. Hellwig, J. Lindner, and S. Kovalev, *Nat. Phys.* **19**, 529 (2023).
- [67] C.-X. Liu, X.-L. Qi, H. Zhang, X. Dai, Z. Fang, and S.-C. Zhang, *Phys. Rev. B* **82**, 045122 (2010).
- [68] T. Low and P. Avouris, *ACS Nano* **8**, 1086 (2014).
- [69] X. Zhang, A. Shkurinov, and Y. Zhang, *Nat. Photon.* **11**, 16 (2017).
- [70] P. Anger, P. Bharadwaj, and L. Novotny, *Phys. Rev. Lett.* **96**, 113002 (2006).
- [71] C. F. Bohren and D. R. Huffman, *Absorption and Scattering of Light by Small Particles* (John Wiley and Sons, New York, 1983).
- [72] N. P. Butch, K. Kirshenbaum, P. Syers, A. B. Sushkov, G. S. Jenkins, H. D. Drew, and J. Paglione, *Phys. Rev. B* **81**, 241301 (2010).
- [73] D. Karaoulanis, E. Paspalakis, and V. Yannopapas, *J. Opt. Soc. Am. B* **38**, 3301 (2021).
- [74] N. Kyvelos, G. Tsigaridas, E. Paspalakis, and V. Yannopapas, *Photonics* **9**, 596 (2022).
- [75] M.-G. Papadaki, N. Kyvelos, E. Paspalakis, and V. Yannopapas, *Photonics* **10**, 658 (2023).
- [76] Y. Tokura, K. Yasuda, and A. Tsukazaki, *Nat. Rev. Phys.* **1**, 126 (2019).

- [77] Y. Zhang, K. He, C.-Z. Chang, C. Li, L. Wang, X. Chen, J. Jia, Z. Fang, X. Dai, W.-Y. Shan, S.-Q. Shen, Q. Niu, X. Qi, S.-C. Zhang, X. Ma, and Q.-K. Xue, *Nature Phys.* **6**, 584 (2009).
- [78] G. D. Chatzidakis and V. Yannopoulos, *Phys. Rev. B* **101**, 165410 (2020).
- [79] M. F. Limonov, M. V. Rybin, A. N. Poddubny, and Y. S. Kivshar, *Nat. Photon.* **11**, 543 (2017).
- [80] A. Canales, D. G. Baranov, T. J. Antosiewicz, and T. Shegai, *J. Phys. Chem.* **154**, 024701 (2021).
- [81] C. Tserkezis, P. E. Stamatopoulou, C. Wolff, and N. A. Mortensen, *Nanophotonics* (2024), [10.1515/nanoph-2023-0781](https://doi.org/10.1515/nanoph-2023-0781), doi: 10.1515/nanoph-2023-0781.
- [82] R. V. Mikhaylovskiy, T. J. Huisman, R. V. Pisarev, T. Rasing, and A. V. Kimel, *Phys. Rev. Lett.* **118**, 017205 (2017).
- [83] I. Thanopoulos, V. Yannopoulos, and E. Paspalakis, *Opt. Lett.* **47**, 5240 (2022).
- [84] J. A. Sobota, S. Yang, J. G. Analytis, Y. L. Chen, I. R. Fisher, P. S. Kirchmann, and Z.-X. Shen, *Phys. Rev. Lett.* **108**, 117403 (2012).
- [85] P. Rießmann, P. Mavropoulos, and S. Blügel, *J. Phys. Chem. Sol.* **128**, 258 (2019).
- [86] L. L. Hale, Z. Wang, C. T. Harris, I. Brener, S. Law, and O. Mitrofanov, *APL Photonics* **8**, 051304 (2023).
- [87] E. A. A. Pogna, L. Viti, A. Politano, M. Brambilla, G. Scamarcio, and M. S. Vitiello, *Nat. Commun.* **12**, 6672 (2021).